# Structural Variation among Retroviral Primer−DNA Junctions: Solution Structure of the HIV-1 (−)-Strand Okazaki Fragment r(gcca)d(CTGC)·d(GCAGTGGC)[†,‡]

Oleg Yu. Fedoroff,[§] Miguel Salazar,[§,||] and Brian R. Reid*[,§,⊥]

*Chemistry and Biochemistry Departments, Box 351700, University of Washington, Seattle, Washington 98195*

*Received April 2, 1996; Revised Manuscript Received June 25, 1996*[⊗]

ABSTRACT: The three-dimensional solution structure of the hybrid−chimeric duplex r(gcca)d(CTGC)·d(GCAGTGGC) has been determined by two-dimensional NMR, restrained molecular dynamics (rMD), and NOE back-calculation methods. This chimera, consisting of a chimeric RNA−DNA strand and its complementary DNA strand, is formed after priming (−)-strand DNA synthesis by $tRNA^{Lys3}$ and subsequent (+)-strand DNA synthesis by reverse transcriptase and is an obligatory intermediate in the formation of double-stranded DNA prior to HIV-1 retrovirus integration. The duplex consists of two different types of double helix: a hybrid form (H-form) and a B-form structure connected by a junction. It is chemically similar to several other Okazaki fragments whose structures have been previously determined in our laboratory. However, some structural parameters are not the same and were found to be sequence dependent. In particular, the sugar conformations at the DNA base pair proximal to the hybrid segment vary from O4′-endo to C2′-endo depending on the base composition. The position of the transition from the relatively wide groove of H-form to the narrow groove of B-form is also sequence dependent, occurring either exactly at the RNA−DNA junction or within the purely DNA segment of the chimera—as is the case in the structure of the present HIV-1 (−)-strand primer. This structural change produces a kink at the DNA−DNA step adjacent to the RNA−DNA junction in the HIV-1 (−)-strand primer. The sequence dependence of structures of RNA−DNA chimeric duplexes may be responsible for the variable cleavage pattern of different Okazaki fragments by reverse transcriptase RNase H.

The human immunodeficiency virus type 1 (HIV-1)[1] is a retrovirus whose mode of replication has been the subject of numerous studies (Kulkoski *et al.*, 1990; Whitcomb *et al.*, 1990; Smith *et al.*, 1990; Pullen & Champoux, 1990; Furfine & Reardon, 1991; Pullen *et al.*, 1992; Peliska & Benkovic, 1992). During the replication of HIV-1 RNA, a double-stranded DNA intermediate is formed, which is flanked at both ends by long terminal repeats (LTRs). At the double-helical DNA level, the LTR sequences are arranged 5′-U3-R-U5, where U5 and U3 are sequences located adjacent to, and unique to, the 5′ and 3′ termini of the viral RNA respectively, and R are sequences derived from the actual viral RNA termini. The action of reverse transcriptase converts the viral RNA into the double-stranded DNA intermediate that is subsequently integrated into the host cell genomic DNA. Following infection of the host cell, the first step in the HIV-1 replication cycle is the synthesis, by reverse transcriptase, of the (−)-strand DNA (cDNA) that is complementary to the single-stranded viral RNA.

Scheme 1

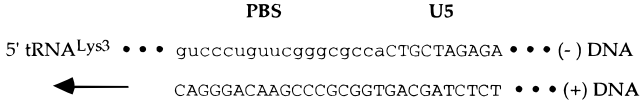


Reverse transcriptase is a DNA polymerase, and as such it requires an RNA primer to initiate DNA synthesis. Synthesis of the (−)-DNA strand by reverse trancriptase is initiated by a cellular tRNA primer, $tRNA^{Lys3}$, which binds to the complementary viral primer binding site (PBS) located near the 5′ end of the HIV-1 RNA genome. After synthesis of the (−)-strand DNA, and during the early stages of (+)-strand DNA synthesis, the chimeric duplex with the sequence shown in Scheme 1 is formed at the PBS−U5 junction (Kulkosky *et al.*, 1990). The lower case letters at the PBS site in Scheme 1 represent RNA residues from the 3 tail of the $tRNA^{Lys3}$ primer. A polypurine-rich RNA fragment (generated by the action of reverse transcriptase RNase H on the viral RNA·cDNA hybrid) primes the synthesis of (+)-strand DNA (Finston & Champoux, 1984). In previous studies of the life cycle of different retroviruses, the deoxynucleotides covalently added to the tRNA primer were found to ultimately define the U5 terminus of the unintegrated viral DNA (Gilboa *et al.*, 1979; Kulkosky *et al.*, 1990; Whitcomb *et al.*, 1990; Pullen *et al.*, 1990). Since all known mature tRNA primers end in a 3′-terminal cca triplet, and

[†] This work was supported by NIH Grants GM-42896 and GM-32681 to B.R.R.

[‡] Coordinates and restraints have been deposited in the Brookhaven Protein Data Bank under the access codes 1GTC and R1GTCMR, respectively.

* To whom correspondence should be addressed at the Department of Chemistry: E-mail, reid@macmail.chem.washington.edu; phone, (206) 685-2331; fax, (206) 685-8665.

[§] Chemistry Department.

[||] Present address: Drug Dynamics Institute, College of Pharmacy, The University of Texas at Austin, Austin, TX 78712.

[⊥] Biochemistry Department.

[⊗] Abstract published in *Advance ACS Abstracts,* August 1, 1996.

[1] Abbreviations: NMR, nuclear magnetic resonance; hybrid, nucleic acid duplex where a pure DNA strand is hydrogen bonded to a DNA strand; chimera, nucleic acid duplex where RNA is covalently bonded to DNA in one or both strands; RT, reverse transcriptase; Mo-MuLV, Moloney murine leukemia virus; HIV-1, human immunodeficiency virus; EDTA, ethylenediaminetetraacetic acid; NOE, nuclear Overhauser effect; 2D, two dimensional; NOESY, nuclear Overhauser effect spectroscopy; rmsd, root mean square deviation; DG, distance geometry; rMD, restrained molecular dynamics.

S0006-2960(96)00782-9 CCC: $12.00 

Scheme 2


since the RNase H enzymes studied at that time (except *Escherichia coli* RNase HI) were found to preferentially cleave RNA−DNA junctions at the ribo−deoxyribo phosphodiester bond (Omer & Faras, 1982; Sawai & Tsukada, 1983; Champoux *et al.*, 1984; Karwan & Wintersberger, 1986; Huber & Richardson, 1990), it was predicted that the right LTR (U5) of the unintegrated HIV-1 viral DNA should start with the 5′ CTGC...3′ sequence shown in Scheme 1. However, more recent studies have shown that the RNase H activity of reverse transcriptase has an unusual specificity in that it cleaves the cytidine−adenosine phosphodiester bond *within* the $tRNA^{Lys}$ primer (Smith & Roth, 1991; Furfine & Reardon, 1991; Pullen *et al*., 1992). Cleavage at this site leaves behind a 5′-terminal riboadenosine residue in the right LTR of the proviral DNA; thus, the sequence of the (−)-strand DNA at the U5 termini is 5′ aCTGC... 3′, and the 5′ nucleotide of the LTR is not the first deoxynucleotide incorporated by extension of an incomplete ...cc-OH $tRNA^{Lys}$ primer, as was originally thought (Kulkoski *et al.*, 1990; Whitcomb *et al.*, 1990; Pullen & Champoux, 1990; Furfine & Reardon, 1991; Pullen *et al*., 1992). This "unusual" RNase H activity, i.e., cleaving exclusively *within* the RNA primer segment, is not restricted to this particular system and has been subsequently found in numerous studies of different RNase H enzymes (Huber & Richardson, 1990; Turchi *et al.*, 1994; Huang *et al.*, 1994).

We became intrigued by the possibility that local sequence-dependent structural perturbations, at or near the cleavage site of RNA−DNA chimeras, might be responsible for the substrate specificity of RNase H. To investigate this idea, we have used two-dimensional NMR (2D-NMR), restrained molecular dynamics (rMD), and NOE back-calculation methods to determine the three-dimensional solution structures of several chimeric duplexes that are cleaved by RNase H in a sequence-dependent fashion. We recently determined the structure of the duplex containing the Moloney murine leukemia virus (−)-strand primer sequence (Salazar *et al*., 1996). Here we report and discuss the structure of a chimeric octamer duplex containing the hybrid−DNA junction derived from Scheme 1 and shown in Scheme 2. An extended form of this junction sequence occurs in nature during the HIV-1 replication life cycle and is believed to be cleaved at the c11−a12 step, one base away from the RNA−DNA junction. As a result of this study we are now able to compare the structures of different chimeric duplexes and to analyze the possible sequence dependence of the structural features that might be responsible for determining the site of RNase H cleavage.

As can be seen from Schemes 1 and 2, the half-hybrid−half-DNA nature of this duplex also makes it an excellent model for the study of Okazaki fragment junction structures. Such fragments are known to occur in lagging-strand synthesis during normal DNA replication (Ogawa & Okazaki, 1980). Recent progress in NMR spectroscopy and chemical synthesis of chimeric RNA−DNA molecules now permits the elucidation of the detailed three-dimensional structures of Okazaki fragments in solution. Previous studies in our laboratory revealed the coexistence of two distinct duplex structural morphologies in a single chimeric duplex, namely, the hybrid form (H-form) in the DNA−RNA segment and a B-form duplex in the pure DNA section; this leads to a pronounced bend at the junction between these two types of duplex morphology (Salazar *et al.*, 1994; Zhu *et al*., 1995). These earlier studies focused on the determination of the structures of chimeric sequences for which the crystal structures were already reported (Wang *et al*., 1982; Egli *et al.*, 1992). In all cases the solution structures were found to be markedly different from the crystal structures. The most probable causes for the discrepancies are the well-documented effects of partial dehydration during crystallization (Kennard & Huber, 1989; Sprous *et al*., 1995) and crystal packing forces (DiGabriele *et al*., 1989) on the nucleic acid crystal structures. It would appear to be important to study the structures of biologically important hybrid and chimeric DNA−RNA duplexes directly in solution.

## MATERIALS AND METHODS

*Sample Preparation.* Ten micromole syntheses of the pure DNA strand and the chimeric RNA−DNA strand were carried out on an automated DNA synthesizer (Applied Biosystems Model 392). The DNA strand was prepared as described previously (Hare *et al*., 1983). The RNA−DNA strand was synthesized by introducing the ribonucleoside phosphoramidites in the appropriate cycles as previously described (Chou *et al*., 1991). Cleavage from the support and base deprotection were carried out with anhydrous methanolic ammonia for 18−24 h. The 2′-TBDMS protecting group was removed from the RNA by dissolving the chimeric strand in a 1 M solution of tetrabutylammonium fluoride (TBAF) in tetrahydrofuran and letting the solution stand overnight at room temperature. Major impurities were then removed by ethanol precipitation. Residual TBAF was removed by ion-exchange column chromatography (AG 50W X-2, Bio-Rad). Further purification was achieved by size exclusion column chromatography (Sephadex DNA grade, superfine, Pharmacia). Column fractions were analyzed by microscale electrophoresis on a 20% polyacrylamide gel and pooled accordingly. The pure DNA and the chimeric strands were then annealed by dissolving equal amounts of each in 500 mM NaCl, 0.2 mM EDTA, and sodium phosphate buffer, pH 6.8, heating to 55 °C, and slowly cooling to room temperature. The sample was subsequently desalted *via* Sephadex G-10 column chromatography. The purified (gccaCTGC)·(GCAGTGGC) duplex (*ca*. 22 mg) was dissolved in 0.4 mL of a buffer consisting of 5 mM KCl, 100 mM NaCl, 0.6 mM EDTA, 25 mM $NaH_2PO_4$, and 25 mM $Na_2HPO_4$, adjusted to pH 7.0. After repeated lyophilization from 99.96% $D_2O$ the sample was finally redissolved in 0.35 mL of 99.996% $D_2O$ for the NMR experiments.

*NMR Spectroscopy.* All NMR experiments were carried out at 26 °C on either a Bruker AM-500 or a home-built 500 MHz NMR spectrometer (Gladden and Drobny, unpublished design). The data were processed on an IRIS 4D computer with either the FTNMR software program (NOESY spectra) or the FELIX software program (E.COSY spectra) from BIOSYM Technologies, San Diego, CA. NOESY spectra were collected in the phase-sensitive hypercomplex mode using 1024 complex points in $t_2$ and 400 pairs of real and imaginary $t_1$ experiments. The NOESY data were

apodized with a 90°-shifted sine-squared function. A relaxation delay of 10 s between scans was used to ensure adequate relaxation of the RNA protons (Wang *et al*., 1992b). The exclusive COSY (E.COSY) spectra were collected in the phase-sensitive TPPI mode. For the E.COSY spectra, maximum sensitivity and resolution in $t_2$ were achieved by acquiring the spectra into 2048 complex points with 48 scans per $t_1$ experiment and sample spinning. A total of 760 $t_1$ experiments were collected. The E.COSY data were processed using 6 Hz of exponential line narrowing and 6 Hz of Gaussian broadening in the $t_2$ and $t_1$ dimensions. Resolution enhancement was achieved by zero-filling to 4096 points in $t_2$ and 2048 points in $t_1$. A proton-detected $^{31}P-^{1}H$ heteronuclear correlation spectrum (Sklenar *et al*., 1986) was collected in the hypercomplex mode with spectral widths of 4386 Hz in the $^{1}H$ dimension and 800 Hz in the $^{31}P$ dimension; 2048 complex points in the $^{1}H$ ($t_2$) dimension and 100 complex points in the $^{31}P$ ($t_1$) dimension were collected. Protons were presaturated for 1.0 s and 256 scans were used for each $t_1$ incrementation. The data were apodized with a 2 Hz exponential line-broadening window function in the $t_2$ dimension and a 90°-shifted sine-squared function in the $t_1$ dimension.

*Structure Determination and Refinement.* All resolved NOESY cross-peaks were integrated over 50, 100, 200, and 400 ms mixing times, and the distances obtained by scaling the initial rates of cross-relaxation to the average initial rate of cross-relaxation for the cytosine H5−H6 proton pairs ($d_{H5-H6}$ = 2.5 Å) were used as initial constraints. For overlapped cross-peaks, an initial lower bound distance was obtained which was subsequently refined by back-calculation of the NOESY spectra. The isotropic tumbling assumption is quite valid for an octamer duplex (Tirado & Garcia de la Torre, 1980; Wang *et al*., 1992a). With the exception of the 5′-terminal residues, all observed cross-peaks were found to be consistent with a single average correlation time for the bases and sugars as monitored by the mutually consistent cross-peaks corresponding to interproton distances that are only very weakly (if at all) dependent on DNA conformation (Reid *et al*., 1989; Fedoroff *et al.*, 1993). We found no evidence for any significant rapid N/S interconversion of the furanose sugar rings in the core of the duplex, particularly in the hybrid section, as some authors have recently suggested (González *et al*., 1994, 1995) (*vide infra*). We did not use *J*-couplings as quantitative constraints for the sugars, since *J*-coupling simulations are compromised to varying extents by neglecting the effects of cross-relaxation on the COSY cross-peak pattern (Harbison, 1993; Zhu *et al*., 1994). Furthermore, we used relatively conservative bounds for the distance constraints which should adequately encompass any uncertainties in the distances arising from the anisotropic effects or the presence of small amplitude internal motions. Initial distance constraints were calculated for each resolved NOESY cross-peak by measuring the initial rate of cross-relaxation and scaling these rates to the average initial rate of cross-relaxation for the resolved cytosine H5−H6 proton pairs ($d_{H5-H6}$ = 2.5 Å). Typical error limits for the upper and lower bound constraints were ±0.2 Å for distances less than 3.5 Å and ±0.3 Å for distances greater than 3.5 Å. An additional 22 distance restraints based on Watson−Crick-type hydrogen bond lengths were included. The backbone conformation was conservatively constrained using a combination of NOESY and qualitative *J*-coupling data as discussed by Kim *et al.* (1992). This approach greatly improves structure convergence by eliminating artificial backbone conformations that contradict the NMR data (Kim *et al*., 1992). The distance constraints were then used as input for distance geometry calculations using the DGII program (BIOSYM Technologies, San Diego, CA) and subsequent restrained molecular dynamics using the DISCOVER program (BIOSYM Technologies, San Diego, CA) with AMBER potential functions (Weiner *et al.*, 1986).

Thirty initial distance geometry structures were generated by embedding the smoothed initial bounds matrix and then were refined by repeated cycles of simulated annealing. After distance geometry, the structures were subjected to a combination of restrained molecular dynamics and conjugate gradient refinement. The force constants in the NOE term used in the DISCOVER program were 30 kcal/(mol Å$^2$). Prior to the molecular dynamics simulations, the structures were first minimized using 2000 cycles of conjugate gradient minimization. The molecular dynamics simulations were then initiated at 300 K with a step size of 1.0 fs for a period of 15 ps using a distance-dependent dielectric constant of 4*r*. A nonbonded cutoff distance of 15 Å was used, and no counterions were included in the simulations. The last coordinate sets were subjected to restrained energy minimization for 2000 steps of conjugate gradient energy refinement. The structure with the lowest energy among these 30 refined structures was then chosen for further iterative refinement of the distance matrix by back-calculation of the NOESY spectra.

The NOESY spectra of the resulting structures were subsequently back-calculated using the improved NOESY simulation program BIRDER (Zhu & Reid, 1995) and an empirically determined correlation time of 4.6 ns. The distance constraints were then adjusted accordingly on the basis of comparison of the calculated and experimental NOE intensities in all spectral regions at 50, 100, 200, and 400 ms mixing times. After the intensities of most of the resolved cross-peaks were reproduced, distance constraints for overlapped cross-peaks were then added in the subsequent stages of iterative refinement. The final set of distance restraints consists of 111 intraresidue, 94 interresidue, and 158 backbone restraints. The NOE *R*-factor ($R = \sum|I_e - I_c|/\sum I_c$, where $I_e$ and $I_c$ are the experimental and the calculated NOE intensities, respectively) was calculated for 96 resolved cross-peaks in the H6/H8−H1′/H2′/H2″/H3′/H4′, the H5−H1′/H2′/H2″, the H1′−H2′/H3′/H4′, and the H2−H1′ regions of the NOESY spectra at 50, 100, 200, and 400 ms—for a total of 384 cross-peak intensities. The DG/rMD/relaxation matrix simulation refinement procedure was repeated until there were no significant improvements in the simulated NOESY spectra and the NOE intensities were reproduced within the signal-to-noise ratio (the noise level corresponds to 20% of cross-peak intensities at 100 ms for distances around 4.0 Å). At the final round of the refinement, 26 out of 30 structures converged to similar values for both the empirical energy and the penalty function for violation of constraints. The remaining four structures had much higher values for both terms and were considered to have not converged. These structures were excluded from the structural analysis.

Table 1: Chemical Shifts (ppm) of the Nonexchangeable Protons and $^{31}$P of r(gcca)d(CTGC)·d(GCAGTGGC) at 26 °C

| residue | H6/H8 | H5/H2/M5 | H1′ | H2′ | H2″ | H3′ | H4′ | $^{31}$P[a] |
|---|---|---|---|---|---|---|---|---|
| 1G | 7.76 | | 5.79 | 2.46 | 2.60 | 4.67 | 4.06 | |
| 2C | 7.32 | 5.25 | 5.62 | 2.03 | 2.36 | 4.74 | 4.08 | −4.21 |
| 3A | 8.04 | 7.37 | 6.02 | 2.66 | 2.77 | 4.87 | 4.29 | −4.00 |
| 4G | 7.21 | | 5.68 | 2.24 | 2.52 | 4.60 | 4.21 | −4.02 |
| 5T | 7.09 | 1.10 | 5.80 | 2.14 | 2.42 | 4.70 | 4.07 | −4.33 |
| 6G | 7.44 | | 5.71 | 2.39 | 2.49 | 4.75 | 4.21 | −4.01 |
| 7G | 7.34 | | 5.84 | 2.34 | 2.52 | 4.68 | 4.24 | −4.00 |
| 8C | 7.17 | 4.94 | 5.96 | 1.93 | 2.09 | 4.30 | 3.90 | −4.16 |
| 9g | 7.66 | | 5.33 | 4.49 | | 4.33 | 4.25 | |
| 10c | 7.63 | | 5.34 | 4.37 | | 4.26 | 4.38 | −4.21 |
| 11c | 7.65 | | 5.25 | 4.45 | | 4.38 | 4.38 | −4.07 |
| 12a | 7.91 | 7.23 | 5.69 | 4.43 | | 4.45 | 4.32 | −3.99 |
| 13C | 7.23 | 5.09 | 5.44 | 1.97 | 2.30 | 4.34 | 4.02 | −4.08 |
| 14T | 7.40 | 1.35 | 5.77 | 1.98 | 2.37 | 4.72 | 4.06 | −4.90 |
| 15G | 7.72 | | 5.80 | 2.41 | 2.54 | 4.82 | 4.21 | −4.37 |
| 16C | 7.27 | 5.21 | 6.01 | 2.01 | 2.04 | 4.34 | 3.90 | −3.98 |

[a] Referenced to trimethyl phosphate as external standard.

## RESULTS

*Analysis of NMR Data.* All protons, except for the geminal H5′/5″ pair, were assigned from NOESY connectivities combined with DQF-COSY and E.COSY data, and the assignments are listed in Table 1. The phosphorus resonances were assigned from the $^{31}$P−$^{1}$H heteronuclear correlation spectrum using sequential H3′−P and P−H4′ cross-peaks. Figure 1A shows the expanded H6/H8 to H1′ region of the NOESY spectrum of r(gcca)d(CTGC)·d(GCAGTGGC) at 200 ms mixing time. The good resolution in this region led to facile assignment of the base to H1′ connectivities for both strands using standard assignment procedures (Hare *et al.*, 1983). Cross-strand NOEs between H1′ protons and adenine H2 protons on the opposite strand, as well as the hydrogen-bonded imino proton spectra (data not shown), indicate that this fragment is double stranded under the conditions of the NMR experiments. Figure 1B shows the expanded H6/H8−H2′/H2″ (DNA) region of the NOESY spectrum of (gccaCTGC)·(GCAGTGGC) at 200 ms mixing time. The intraresidue H6/H8 to H2′/H2″ NOEs are connected by vertical lines, and the H6/H8-H2′ peaks are labeled with the residue number. There is significant overlap for the intra- and interresidue NOEs for residues 2C, 7G, and 6G, but some interesting qualitative patterns emerge for the well-resolved cross-peaks. First, the intraresidue H6/H8−H2′ NOEs are the most intense, and this is particularly true for residue 3A which was found to have higher sugar pseudorotation *P* values (*vide infra*). Second, in contrast to observations in "normal" DNA duplexes, the internucleotide (*n*)H6/H8−(*n*−1)H2″ cross-peaks are not much stronger than the intranucleotide (*n*)H6/H8−(*n*)H2″ cross-peaks. These observations suggest a somewhat different geometry for the sugar residues in the DNA strand than that found in B-form DNA and perhaps also a quite different spatial relationship between adjacent nucleotides. Note that the intranucleotide (*n*)H6/H8−(*n*)H2″ cross-peaks for residues 13C and 4G are significantly weaker than those of other well-resolved cross-peaks, indicating a lower *P* value for the sugars of these residues. This is consistent with the *P* values deduced from the coupling constants of these sugar residues (Salazar *et al.*, 1993). Finally, strong internucleotide (*n*)H6/H8−(*n*−1)H2′ cross-peaks were observed for the junction DNA residue C13 and the RNA residues c10, c11, and a12 (Figure 1c). These strong NOEs, corresponding to interproton distances shorter than 2.5 Å, are characteristic of A-form geometry and directly indicate the heteromerous nature of this chimeric duplex.

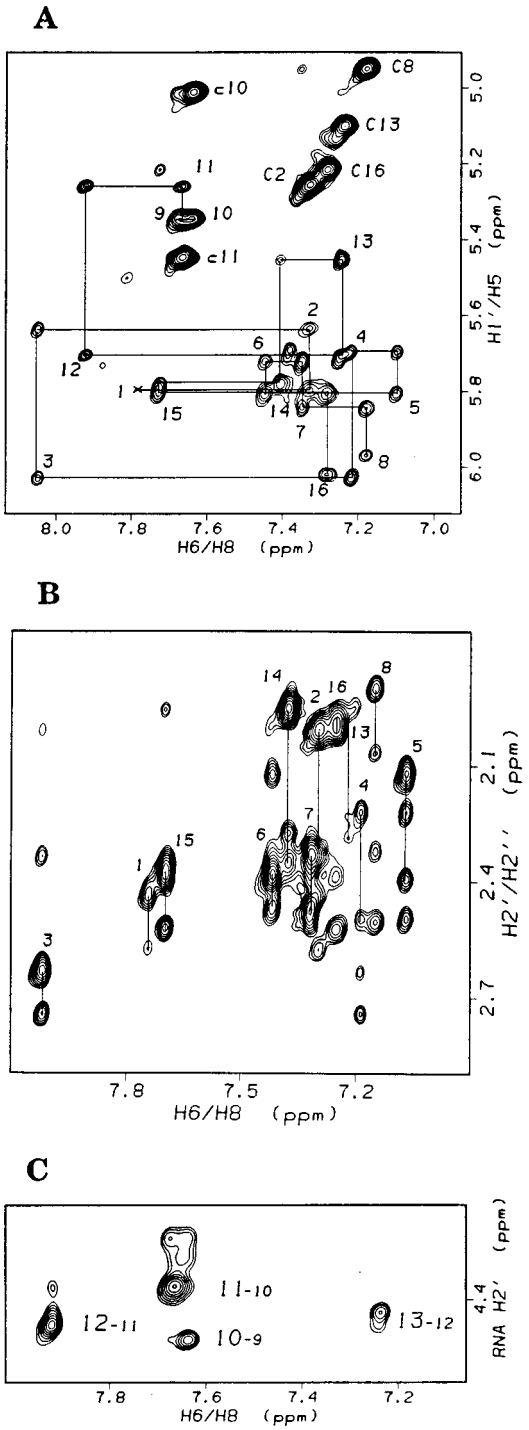


FIGURE 1: Assignment of (A) the RNA/DNA H6/H8−H1′, (B) the DNA H6/H8−H2′/H2″ (B) (top), and (C) the RNA H6/H8−H2′ regions of the NOESY spectra of r(gcca)d(CTGC)·d(GCAGTGGC). The (*n*)H6/H8−(*n*)H2′ cross-peaks in spectrum B are labeled and are connected to the (*n*)H6/H8−(*n*)H2″ cross-peaks by solid vertical lines. The (*n*)H6/H8−(*n*)H1′ cross-peaks in A are labeled with the residue number according to the numbering scheme shown in the text. The terminal 1GH8−1GH1′ NOE (indicated with an "x") is modulated by motional end effects, and the cross-peak is only visible at lower contour levels. The contour level in (C) is much higher than in (A) and (B) so only the strongest RNA cross-peaks are visible. The H6/H8 shifts of (*n*)H6/H8−(*n*−1)H2′ cross-peaks are designated by larger numbers and the H2′ by smaller residue numbers.

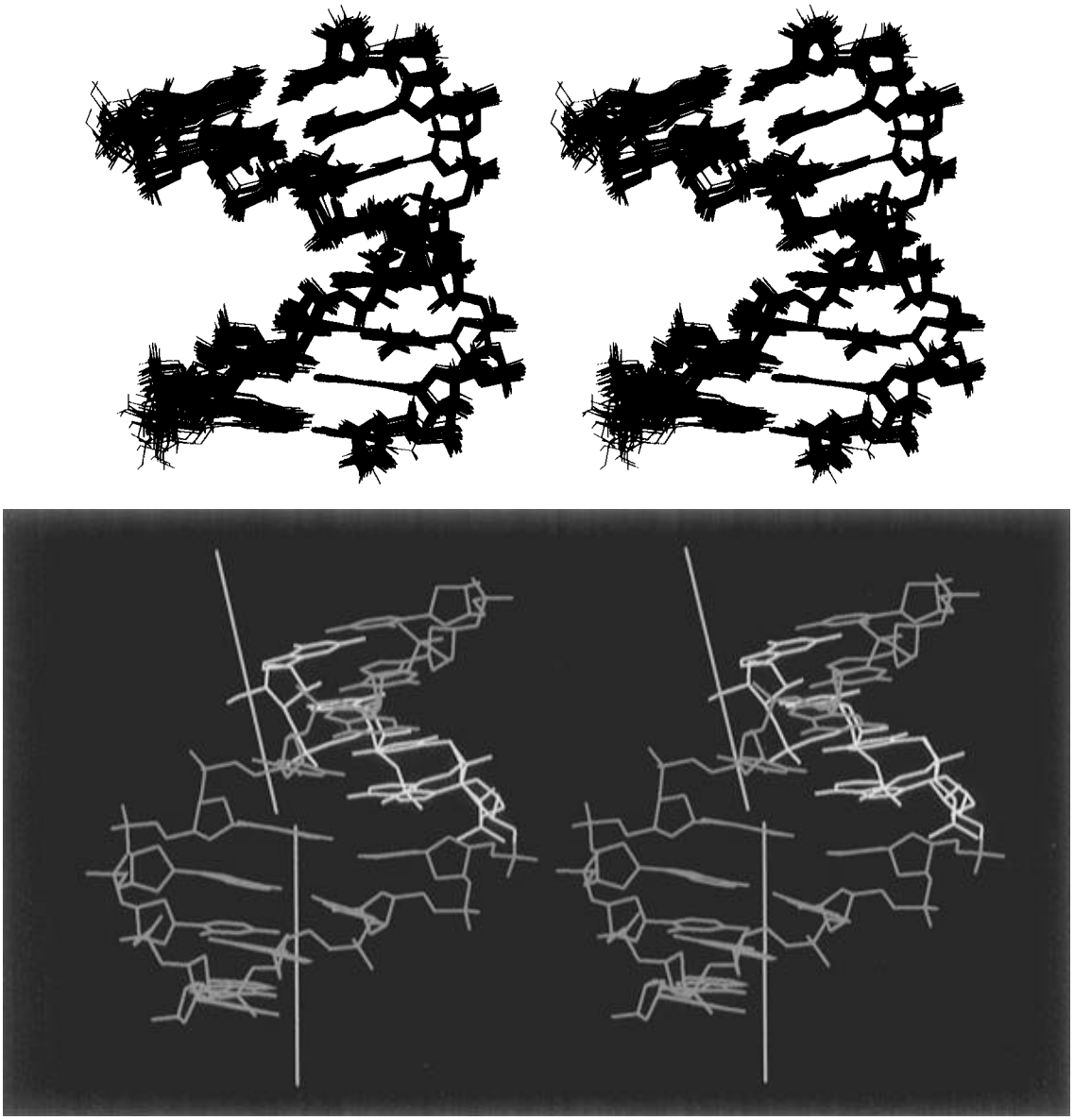

FIGURE 2: (A, top) Superimposed stereoviews of the 26 final DG/rMD structures of the HIV-1 retroviral junction fragment r(gcca)d-(CTGC)·d(GCAGTGGC). All these structures have pairwise rmsd values within the range 0.6 ± 0.3 Å. (B, bottom) Stereoview of one of the final structures at ~90° rotation relative to panel A. The DNA residues are shown in blue and the RNA residues in white. Two helical axes (yellow) for the hybrid and DNA parts illustrate the 16° bend in the structure (the standard deviation of the bending angle is 3°). Note the 25° kink at the DNA step next to the RNA−DNA junction.

*Structural Features of (gccaCTCG)·(GCAGTGGC).* Twenty-six structures were generated separately from the refined distance bounds by embedding and refinement (see Materials and Methods). Table 2 summarizes the refinement statistics. All refined structures superimpose quite well (Figure 2A), reflecting small rmsd values between them (Table 2). Thus multiple independent structure determinations reliably produce essentially the same well-defined conformation shown in Figure 2B. Two different helical axes for the upper and lower halves of the molecule illustrate the bend between the hybrid segment and the pure DNA segment. Figure 3 shows a comparison of the experimental and the simulated H6/H8 to H1′ (below) and H2′/H2″ (above) regions of the NOESY spectrum of one of the final refined octamer structures at 100 ms mixing time. The good agreement between the simulated and experimental spectra is evident and merely reflects graphically the low NOE *R*-factors (Table 2).

Table 2: NOE *R*-Factors and Energy Analysis (in kcal/mol) of the Final Structures Obtained from Distance Geometry/Restrained Molecular Dynamics/NOESY Back-Calculation Refinement in AMBER Force Field

| energy terms | energy value |
|---|---|
| total energy[a] | −127.65 ± 3.21 |
| bond | 7.35 ± 0.20 |
| angle | 65.68 ± 1.16 |
| dihedral | 150.51 ± 2.22 |
| hydrogen bond energy | −13.39 ± 0.12 |
| nonbond energy | −160.12 ± 1.44 |
| nonbond repulsion energy | 519.92 ± 2.01 |
| nonbond dispersion energy | −680.03 ± 2.82 |
| Coulomb energy | −177.77 ± 0.52 |
| distance forcing potential energy[b] | 20.13 ± 1.08 |
| NOE *R*-factor[c] | 0.23 ± 0.02 |

[a] Includes small contribution (~0.05 kcal/mol) from out-of-plane energy terms. [b] This contribution has been subtracted from the total energy. [c] The NOE *R*-values are calculated for 96 resolved cross-peaks at four different mixing times.

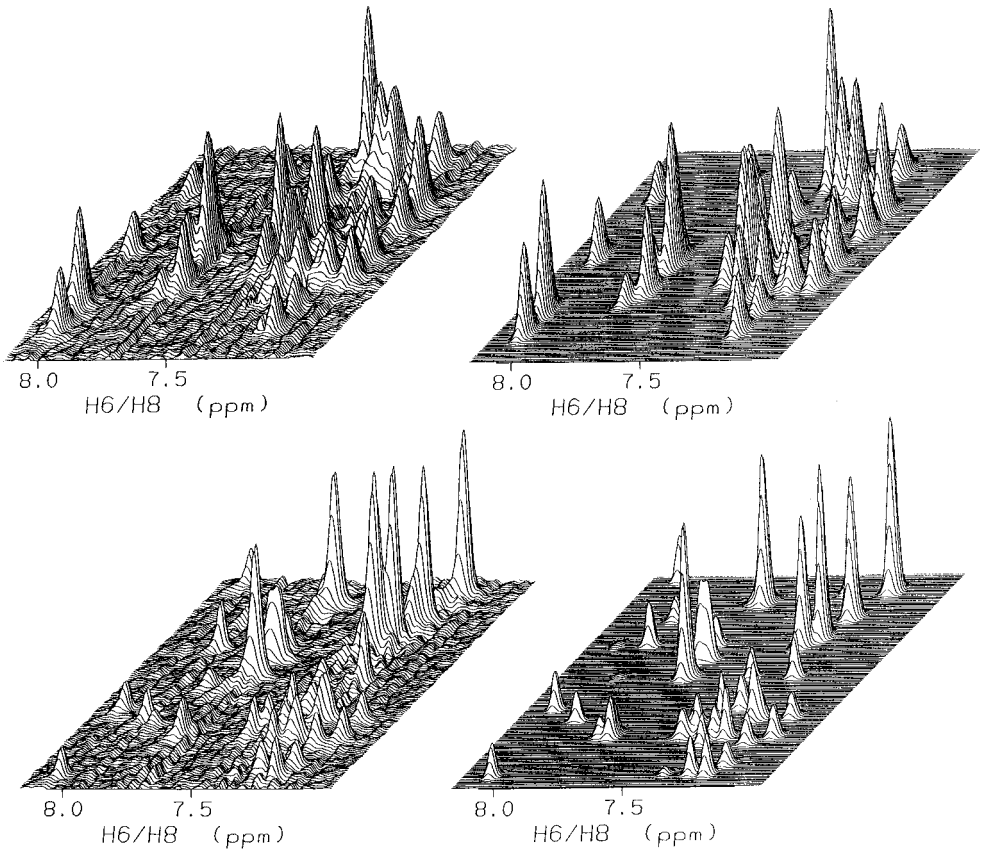


FIGURE 3: Stack plots of the experimental (left column) and back-calculated (right column) H6/H8 to H1′/H2′/H2″ NOESY spectra for one of the refined chimeric structures. The DNA H6/H8−H2′/H2" and the RNA/DNA H6/H8−H1′ NOESY cross-peaks are shown in the top and bottom rows, respectively.

The sugar conformations in this chimeric duplex were analyzed previously in our earlier study of sugar proton *J*-couplings (Salazar *et al.*, 1993a). In that study we came to the conclusion that the RNA sugars have C3′-endo conformations [phase angle (*P*) in the 0−40° range] while the DNA sugars have conformations between O4′-endo and C2′-endo (*P* is between 60° and 150°) with particularly low P values for the junction DNA residues. As can be seen from Figure 4, these values are in quite good agreement with the present NOE-derived solution structure. The anomalously low *P* values for the junction residues (∼110° for G4 and ∼90° for c13) are especially interesting since, in the Mol-MuLV (−)-primer, the corresponding DNA residues have "normal" C2′-endo conformations (Salazar *et al.*, 1996). Therefore, the transition from H-form in the hybrid section to the B-form in the DNA section is more localized in the case of the Mol-MuLV primer and may influence the interaction of RNase H with this chimeric substrate.

RT RNase H is an endonuclease without exonucleolytic activity (Krug & Berger, 1989). This implies a requirement for RNase H interaction with the duplex on the 3′ side of the cleavage site. Interestingly, it is the DNA−DNA step next to the RNA−DNA junction step that is the site of a major structural distortion in the HIV-1 (−)-strand primer. In contrast to the Mo-MuLV primer, there is a 25° tilt-type kink at this step (Figures 2b and 5) which is accomplished by a profound change in the value of the α backbone angle (Figure 4). The conformation of the sugar−phosphate backbone is defined by the torsion angles α, $\beta$, $\gamma$, $\delta$, $\epsilon$, and $\zeta$, with α corresponding to the P → O5′ rotation and $\zeta$ corresponding to the O3′ → P rotation (Saenger, 1984). The phosphorus chemical shift is sensitive to the rotation angles about these P−O ester bonds α and $\zeta$ (Gorenstein & Kar, 1975). The $^{31}$P−$^{1}$H heteronuclear correlation spectrum for the HIV-1 (−)-strand primer is shown in Figure 6. The $^{31}$P resonance of the 13C−14T step is shifted upfield from the other $^{31}$P resonances (Figure 6). This shift is qualitatively consistent with the value of the P−O5′ torsional angle α close to 300°, which corresponds to the maximal upfield shift for $^{31}$P resonances (Gorenstein & Kar, 1975). No analogously upfield-shifted $^{31}$P resonance exists for the Mo-MuLV (−)-primer (data not shown), in agreement with the NOE-derived structures (Figures 4 and 5).

The O3′−P torsional angle $\zeta$ is very different in $B_I$ and $B_{II}$ backbone conformations (Fratini *et al.*, 1982) and contributes as much as α to the $^{31}$P chemical shift (Gorenstein & Kar, 1975; Gorenstein *et al.*, 1988). The absence of strongly downfield-shifted $^{31}$P resonances is consistent with normal $B_I$ conformations for all steps, including the RNA−DNA junction (Chou *et al.*, 1992). One can expect that higher $\zeta$ values for RNA residues (Figure 4) should also manifest themselves in upfield-shifted $^{31}$P resonances. However, the lower values of the α torsional angle for RNA residues (Figure 4) offset this effect, and RNA and DNA $^{31}$P resonances have similar chemical shifts (Figure 6). $^{31}$P−$^{1}$H heteronuclear correlation experiments can also provide information about $J_{H3'-P}$ coupling, which is related to the H3′−C3′−O3′−P torsion angle (Lankhorst *et al.*, 1984) and can be used for estimating the $\epsilon$ torsion angle C3′ → O3′ (Sklenar & Bax, 1987; Gorenstein *et al.*, 1988). Several experiments have been designed for accurate measurement of $J_{H3'-P}$ couplings in DNA fragments by semiselectively

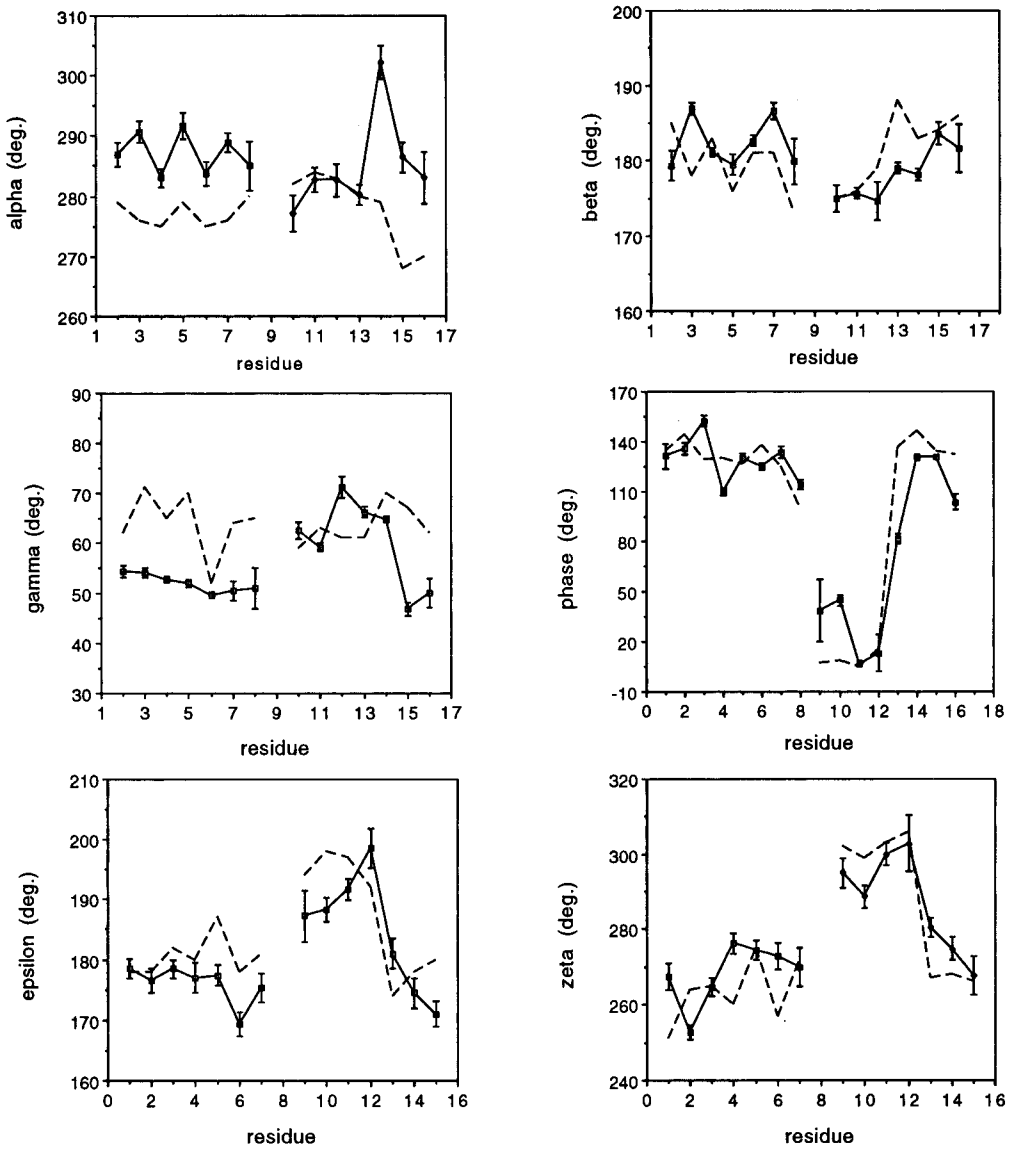


FIGURE 4: Backbone torsional angles and sugar puckers for the final structures of r(gcca)d(CTGC)·d(GCAGTGGC) compared to the corresponding values (broken line) of the solution structure of r(ccca)d(AATGA)·d(TCATTTGGG) (Salazar *et al*., 1996). The sequences were aligned with respect to the RNA−DNA junction. Error bars illustrate standard deviations for the ensemble of the 26 final structures shown in Figure 2A.

suppressing homonuclear couplings to the H3′ protons (Sklenar & Bax, 1987). Unfortunately, the upfield chemical shifts of the RNA and some DNA H3′ protons in the RNA−DNA chimera limit the usefulness of these experiments in this particular case. However, $J_{H3'-P}$ couplings can be qualitatively estimated from the $^{31}P-^{1}H$ heteronuclear correlation experiment by subtracting the passive $^{1}H-^{1}H$ couplings from the total width of the $^{31}P-H3'$ multiplets (Varani *et al*., 1991). Following this procedure, we estimate that the RNA H3′−P couplings are consistently stronger than the DNA P−H3′ couplings by 3−5 Hz and, according to the Karplus relationship, should correspond to higher values of the $\epsilon$ torsion angle in the $B_I$ conformation (Kim *et al*., 1992). This is in agreement with the $\epsilon$ values in the refined structures (Figure 4). Very large splitting of the RNA H3′−P cross-peaks is also evident directly from Figure 6.

Another interesting difference between HIV-1 and Mo-MuLV Okazaki fragments is the variation in buckle along the sequence (Figure 5). While in the Mo-MuLV chimera the base pair with the largest negative buckle is the junction 5·12 RNA−DNA pair; in the HIV-1 chimera the situation is quite different. The base pairs with largest negative buckle are now the 4·13 junction base pair and the 6·11 hybrid base pair one step removed from the junction. The cup values, which are essentially the difference between buckles of successive base pairs, are also very different (Figure 5). In the Mo-MuLV primer the junction step has a negative cup, and the adjoining hybrid step has a positive cup. The reverse is true for the HIV-1 primer; the junction step has a positive cup value, and the neighboring hybrid step has a negative cup. Even more interesting is the difference in the minor groove width (Figure 7). The Mo-MuLV primer−product junction has a consistently narrower minor groove throughout all steps except the terminal one. This may be due to the presence of an $A_nT_m$ tract, which is known to cause minor groove compression in DNA when $n + m > 3$ (Chuprina *et al*., 1991b). Such a structural distortion involves the junction step in this case. In contrast, the HIV-1 primer chimera has a rather uniform minor groove width across the hybrid section, and the transition to B-form structure takes place completely within the DNA section. As a consequence, the difference in minor groove width between these two different

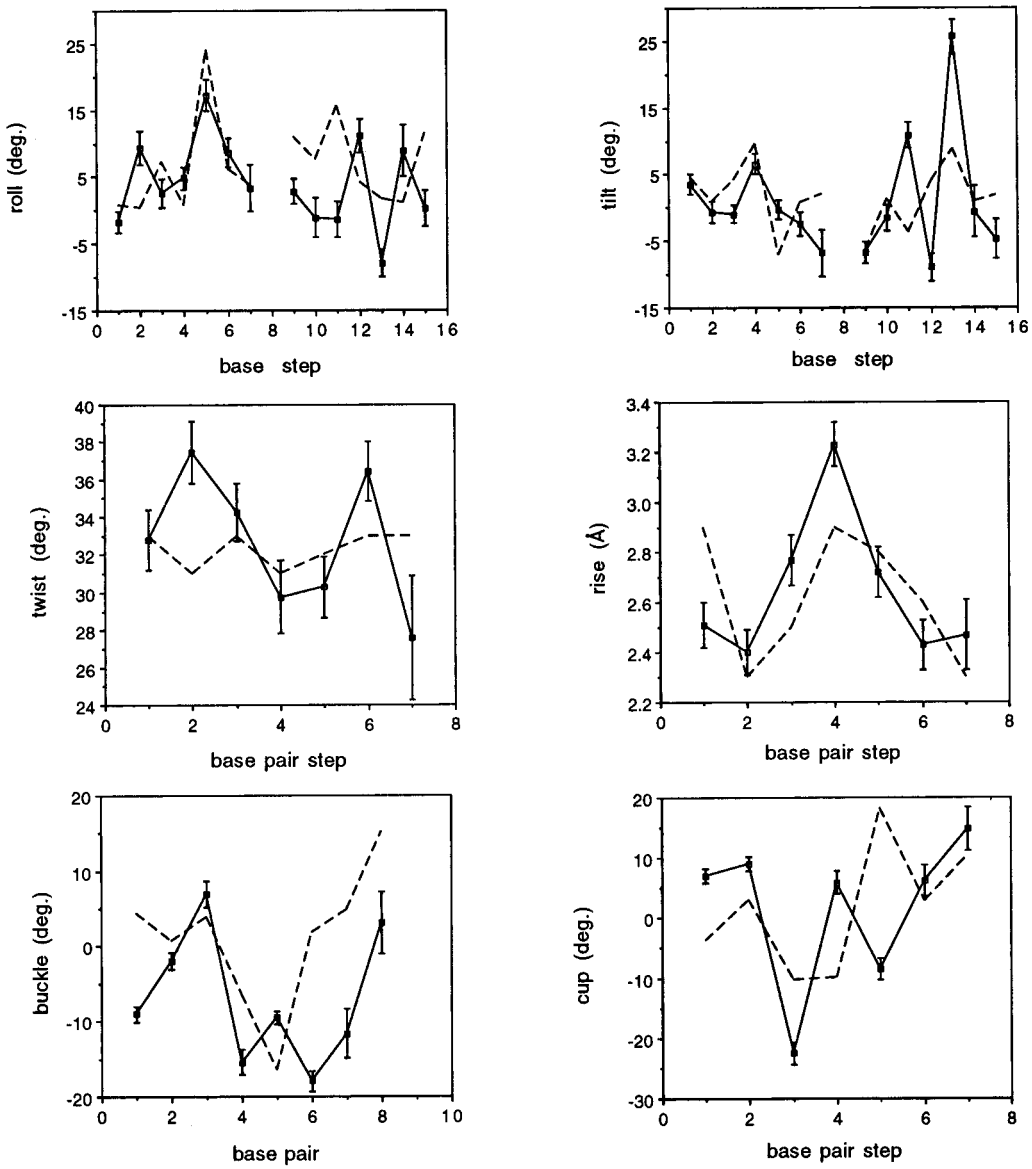


FIGURE 5: Selected structural parameters of the final structures of r(gcca)d(CTGC)·d(GCAGTGGC) compared to the corresponding values (broken line) of the solution structure of r(ccca)d(AATGA)·d(TCATTTGGG) (Salazar *et al.*, 1996). The helical parameters were calculated using the program NEWHEL93 (R. E. Dickerson, UCLA). The sequences were aligned with respect to the RNA−DNA junction. Error bars illustrate standard deviations for the ensemble of the 26 final structures shown in Figure 2A.

chimeric sequences reaches 1.5 Å at the RNA−DNA junction step, which in turn can affect their interaction with RNase H.

## DISCUSSION

The junction between the hybrid sections and pure DNA sections of Okazaki fragments is an exceptionally good target for all retroviral and eukaryotic RNase H enzymes studied so far. Usually RNase H makes a single cleavage exactly at the covalent junction, or one RNA base away from it, and leaves the remaining RNA primer essentially intact (Omer & Faras, 1982; Sawai & Tsukada, 1983; Champoux *et al.*, 1984; Karwan & Wintersberger, 1986; Huber & Richardson, 1990; Smith & Roth, 1991; Furfine & Reargon, 1991; Pullen *et al.*, 1992; Huber & Richardson, 1990; Eder *et al.*, 1993; Turchi *et al.*, 1994; Huang *et al.*, 1994). It was suggested that, in contrast to *E. coli* RNase H, the analogous enzymes that operate in eukaryotic cells are "designed to recognize the initiator RNA of Okazaki fragments" (Turchi *et al.*, 1994). It is of special interest to determine the structural characteristics of both the enzyme (RNase H) and the substrate (Okazaki fragment) that are responsible for such behavior.

Recently, we have shown that the major structural determinant of RNase H specificity appears to be the minor groove width of RNA−DNA duplexes (Fedoroff *et al.*, 1993). Specifically, it is the unique shape and width of the minor groove of hybrid duplexes which allows RNase H to discriminate between hybrid duplexes and pure RNA duplexes. The consensus structural feature of HIV-1 and Mo-MuLV (−)-strand primer-product chimeras is the relatively narrower minor groove width in their hybrid section compared to the groove width of all RNA−DNA hybrid duplexes studied so far (Fedoroff *et al.*, 1993; Salazar *et al.*, 1993b; Lane *et al.*, 1993; Gonzales *et al.*, 1995). Thus, it is possible that the same mechanism of RT RNase H specificity—sensitivity to the minor groove width—may also be responsible for the specific cleavage of Okazaki fragments.

The right-handness of the double helix and the minor-groove binding mode of RNase H dictate that the enzyme

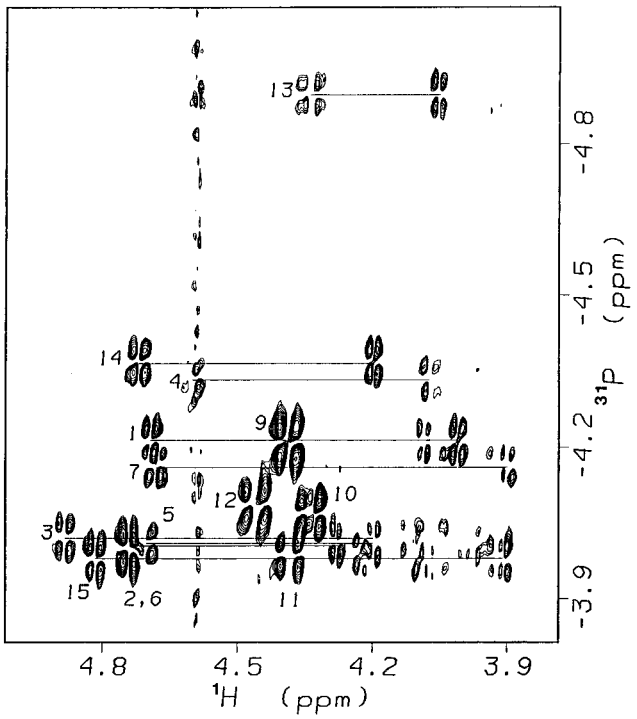


FIGURE 6: Proton-detected $^{31}$P−$^{1}$H heteronuclear correlation spectrum of the r(gcca)d(CTGC)·d(GCAGTGGC) chimera. (*n*)$^{31}$P−(*n*-1)H3′ cross-peaks are labeled with the residue numbers of H3′ protons. The horizontal lines connect the DNA (*n*)$^{31}$P−(*n*−1)H3′ and (*n*)$^{31}$P−(*n*)H4′ cross-peaks. The RNA (*n*)$^{31}$P−(n)H4′ cross-peaks are very weak due to the multiplet cancellation by the strong RNA H3′−H4′ passive couplings and cannot be seen at this contour level.

must contact residues of the hybrid section DNA strand located two to three residues downstream (3′) from the DNA residue opposite the cleavage site (Wyatt & Walker, 1989; Nakamura *et al*., 1991). However, the residues of the B-form pure DNA section of the Okazaki fragment are located in the opposite direction from the cleavage site and most likely influence RNase H binding indirectly, by modulating the minor groove width at or near the junction. For example, the structural distortion at the DNA step next to the RNA−DNA junction in the HIV-1 (−)-strand primer results in a substantially wider minor groove at the junction compared to the minor groove in the Mo-MuLV chimera (Figure 7).

It is also possible that the actual structural element of the Okazaki fragment that is recognized by RT RNase H is the prominent bend in the double helix between the hybrid and DNA segments. Indeed, the pure DNA duplex is strongly bent in the crystal structure of a complex of DNA with HIV-1 RT (Jacobo-Molina *et al*., 1993), and the DNA has a structure very similar to the solution structure of an Okazaki fragment (Salazar *et al*., 1994). The influence of double-helix bending on DNA and RNA interactions with proteins is well documented (Goodman & Nash, 1989; Gartenberg & Crothers, 1991; Kahn & Crothers, 1992; Lesser *et al*., 1993; Marino *et al*., 1995) and should be taken into account in the case of such strongly bent molecules as Okazaki fragments. The present structure has a bending angle (≈16°) close to that of the analogous Okazaki fragments gcgTATACCC·GGGTATACGC (≈18°) (Salazar *et al*., 1994) and the Mo-MuLV primer r(ccca)d(AATGA)·d(TCATTTGGG) (≈21°) (Salazar *et al*., 1996) and in the self-complementary cgcgTATACGCG duplex (≈21°) (Zhu *et al*., 1995). There is a strong dependence of the magnitude of bending on the gradient of the minor groove width change in pure DNA duplexes (Chuprina *et al*., 1991a,b). Such a coupling of bending and minor groove width change is also valid for the RNA−DNA junction: the very big change in the minor groove width from 8 Å in the hybrid section to 5 Å inside the DNA segment (Figure 7) is accompanied by pronounced bending of the double helix (Figure 2B).

The main focus of the current work was the three-dimensional structures of retroviral Okazaki fragments. Both Mo-MuLV and HIV-1 (−)-strand primers show prominent structural changes in and around the RNA−DNA junction. Both primers are cleaved predominantly at the same site, i.e., one base removed from the chemical junction, but there are some data indicating that the Mo-MuLV primer can also be cleaved exactly at the junction by HIV-1 RT RNase H, although at a lower level (Schultz et al., 1995). There is a possibility that the narrow minor groove of the Mo-MuLV primer at the RNA−DNA junction step is responsible for such mixed cleavage specificity. We can only anticipate the variations in the structures of other Okazaki fragments, such as (+)-strand primers, which are cleaved at the junction by RT RNase H enzymes (Champoux *et al*., 1984; Huber & Richardson, 1990), and these will be the subject of future studies.

Finally, besides the fundamental interest in the structure of such duplexes, there is a potential benefit to antisense

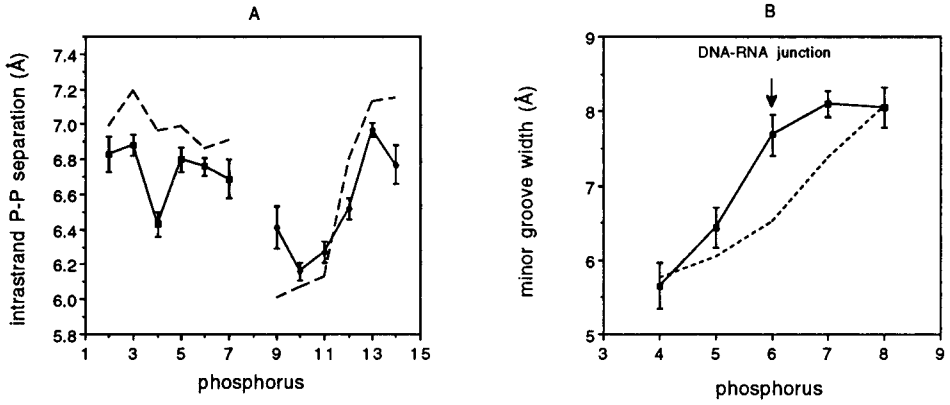


FIGURE 7: Intrastrand phosphorus−phosphorus distances (A) and minor groove widths (B) for the final r(ccca)d(AATGA)·d(TCATTTGGG) duplex solution structures. Broken lines show the corresponding values for the recently determined solution structure of the chimeric Mo-MulV duplex r(ccca)d(AATGA)·d(TCATTTGGG) (Salazar *et al*., 1996). Phosphorus atoms are numbered according to Saenger (1984); i.e., G1 and g9 have no phosphate group. The phosphorus numbering of Mo-MulV chimera was aligned with respect to the RNA−DNA junction. The minor groove width was calculated by subtracting 5.8 Å from the cross-strand phosphorus−phosphorus distances.

technology. RNase H activity is very important for the antisense effect of oligonucleotides designed to suppress the expression of pathogen genes. Particularly, oligonucleotides with backbone and sugar modifications that interfere with RNase H binding usually show less potency than oligonucleotides that evoke RNase H-mediated cleavage of the target RNA molecule (Cazenave *et al*., 1989; Boiziau *et al*., 1992; Monia *et al*., 1993). To capitalize on this mechanism of antisense action, one should take into account the fact that although mammalian RNase HI cleaves hybrid RNA−DNA duplexes, it cleaves chimeric Okazaki fragments much more readily (Eder *et al*., 1993; Huang *et al*., 1994). One aspect of the present study was to determine structural features responsible for this effect. We believe that such knowledge should help in the design of antisense oligonucleotides with increased potency.

## ACKNOWLEDGMENT

We thank Ms. Julie M. Miller for her assistance in the purification of the chimeric duplex, Dr. Leiming Zhu for the use of his improved back-calculation program BIRDER, and Dr. James J. Champoux and members of his laboratory for illuminating discussions and communicating their results before publication.

## REFERENCES

Boiziau, C., Thuong, N. T., & Toulmé, J.-J. (1992) *Proc. Natl. Acad. Sci. U.S.A. 89*, 768−772.
Cazenave, C., Stein, C. A., Loreau, N., Thuong, N. T., Neckers, L. M., Subasinghe, C., Hélène, C., Cohen, J. S., & Toulmé, J.-J. (1989) *Nucleic Acids Res. 17*, 4255−4273.
Champoux, J. J., Gilboa, E., & Baltimore, D. (1984) *J. Virol. 49*, 686−691.
Chuprina, V. P., Fedoroff, O. Yu., & Reid, B. R. (1991a) *Biochemistry 30*, 561−568.
Chuprina, V. P., Lipanov, A. A., Fedoroff, O. Yu., Kim, S.-G., Kintanar, A., & Reid, B. R. (1991b) *Proc. Natl. Acad. Sci. U.S.A. 88*, 9087−9091.
DiGabriele, A. D., Sanderson, M. R., & Steitz, T A. (1989) *Proc. Natl. Acad. Sci. U.S.A. 86*, 1816−1820.
Eder, P. S., Walder, R. Y., & Walder, J. A. (1993) *Biochimie 75*, 123−126.
Egli, M., Usman, N., Zhang, S., & Rich, A. (1992) *Proc. Natl. Acad. Sci. U.S.A. 89*, 534−538.
Egli, M., Usman, N., & Rich, A. (1993) *Biochemistry 32*, 3221−3237.
Fedoroff, O. Y., Salazar, M., & Reid, B. R. (1993) *J. Mol. Biol. 233*, 509−523.
Finston, W. I., & Champoux, J. J. (1984) *J. Virol. 51*, 26−33.
Fratini, A. V., Kopka, M. L., Drew, H. R., & Dickerson, R. E. (1982) *J. Biol. Chem. 257*, 14686−14707.
Furfine, E. S., & Reardon, J. E. (1991) *Biochemistry 30*, 7041−7046.
Gartenberg, M. R., & Crothers, D. M. (1991) *J. Mol. Biol. 219*, 217−230.
Gilboa, E., Mitra, S. W., Goff, S., & Baltimore, D. (1979) *Cell 18*, 93−100.
González, C., Stec, W., Kobylanska, A., Hogrefe, R. I., Reynolds, M., & James, T. L. (1994) *Biochemistry 33*, 11062−11072.
González, C., Stec, W., Reynolds, M., & James, T. L. (1995) *Biochemistry 34*, 4969−4982.
Goodman, S. D., & Nash, H. (1989) *Nature 341*, 251−254.
Gorenstein, D. G., & Kar, D. (1977) *J. Am. Chem. Soc. 99*, 672−677.
Gorenstein, D. G., Schroeder, S. A., Fu, J. M., Metz, J. T., Roonta, V., & Jones, C. R. (1988) *Biochemistry 27*, 7223−7237.
Harbison, G. S. (1993) *J. Am. Chem. Soc. 115*, 3026−3027.
Hare, D. R., Wemmer, D. E., Chou, S. H., Drobny, G., & Reid, B. R. (1983) *J. Mol. Biol. 171*, 319−336.
Huang, L., Kim, Y., Turchi, J. J., & Bambara, R. A. (1994) *J. Biol.Chem. 269*, 25922−25927.
Huber, H. E., & Richardson, C. C. (1990) *J. Biol. Chem. 265*, 10565−10573.
Jacobo-Molina, A., Ding, J., Nanni, R. G., Clark, A. D., Jr., Lu, X., Tantillo, C., Williams, R. L., Kamer, G., Ferris, A. L., Clark, P., Hizi, A., Hughes, S. H., & Arnold, E. (1993) *Proc. Natl. Acad. Sci. U.S.A. 90*, 6320−6324.
Kahn, J. D., & Crothers, D. M. (1992) *Proc. Natl. Acad. Sci. U.S.A. 89*, 6343−6347.
Karwan, R., & Wintersberger, U. (1986) *FEBS Lett. 206*, 189−192.
Kennard, O., & Hunter, W. N. (1989) *Q. Rev. Biophys. 22*, 327−379.
Kim, S.-G., Lin, L.-J., & Reid, B. R. (1992) *Biochemistry 31*, 3564−3574.
Krug, M. S., & Berger, S. L. (1989) *Proc. Natl. Acad. Sci. U.S.A. 86*, 3539−3543
Kulkosky, J., Katz, R. A., & Skalka, A. M. (1990) *J. Acquired Immune Defic. Syndr. 3*, 852−858.
Lane, A. W., Ebel, S., & Brown, T. (1993) *Eur. J. Biochem. 215*, 297−306.
Lesser, D. R., Kurpiewski, M. R., Waters, T., Connolly, B. A., & Jen-Jacobson, L. (1993) *Proc. Natl. Acad. Sci. U.S.A. 90*, 7548−7552.
Marino, J. P., Gregorian, R. S., Jr., Csankovszki, G., & Crothers, D. M. (1995) *Science 268*, 1448−1454.
Mitra, S. W., Chow, M., Champoux, J. J., & Baltimore, D. (1982) *J. Biol. Chem. 257*, 5983−5986.
Monia, B. P., Lesnik, E. A., Gonzales, C., Lima, W. F., McGee, D., Guinosso, C. J., Kawasaki, A. M., Cook, P. D., & Freier, S. M. (1993) *J. Biol. Chem. 268*, 14514−14522.
Muesing, M. A., Smith, D. H., Cabradilla, C. D., Benton, C., Lasky, L., & Capon, D. (1985) *Nature 313*, 450−458.
Nakamura, H., Oda, S., Iwai, S., Inoue, H., Ohtsuka, E., Kanaya, S., Kimura, S., Katsuda, C., Katayanagi, K., Morikawa, K., Miyaashiro, H., & Ikehara, M. (1991) *Proc. Natl. Acad. Sci. U.S.A. 88*, 11535−11539.
Ogawa, T., & Okazaki, T. (1980) Discontinuous DNA replication, *Annu. Rev. Biochem. 49*, 421−457.
Omer, C. A., & Faras, A. J. (1982) *Cell 30*, 797−805.
Peliska, J. A., & Benkovic, S. (1992) *Science 258*, 1112−1118.
Pullen, K. A., & Champoux, J. J. (1990) *J. Virol. 64*, 6274−6277.
Pullen, K. A., Ishimoto, L. K., & Champoux, J. J. (1992) *J. Virol. 66*, 367−373.
Rattray, A. J., & Champoux, J. J. (1987) *J. Virol. 61*, 2843−2851.
Resnick, R., Omer, C. A., & Faras, A. J. (1984) *J. Virol. 51*, 813−821.
Saenger, W. (1984) *Principles of Nucleic Acids Structure*, Springer, New York.
Salazar, M., Champoux, J. J., & Reid, B. R. (1993a) *Biochemistry 32*, 739−744.
Salazar, M., Fedoroff, O. Y., Miller, J. M., Ribeiro, N. S., & Reid, B. R. (1993b) *Biochemistry 32*, 4207−4215.
Salazar, M., Fedoroff, O. Y., Zhu, L., & Reid, B. R. (1994) *J. Mol. Biol. 241*, 440−455.
Salazar, M., Fedoroff, O. Y., & Reid, B. R. (1996) *Biochemistry 35*, 8126−8135.
Sawai, Y., & Tsukada, K. (1983) *Biochem. Biophys. Res. Commun. 110*, 470−476.
Schultz, S. J., Whitting, S. H., & Champoux, J. J. (1995) *J. Biol. Chem. 270*, 24135−24145.
Schwartz, D. E., Tizard, R., & Gilbert W. (1983) *Cell 32*, 853−869.
Sclenar, V., & Bax, A. (1987) *J. Am. Chem. Soc. 109*, 7525−7526.
Sclenar, V., Miyashiro, H., Zon, G., Miles, H. T., & Bax, A. (1986) *FEBS Lett. 208*, 94−98.
Shinnick, T. M., Lerner, R. A., & Sutcliffe, J. G. (1981) *Nature 293*, 543−548.
Shoemaker, C., Goff, S., Gilboa, E., Paskind, M., Mitra, S. W., & Baltimore, D. (1980) *Proc. Natl. Acad. Sci. U.S.A. 77*, 3932−3936.
Smith, J. S., & Roth, M. J. (1992) *J. Biol. Chem. 267*, 15071−15079.
Smith, J. S., Kim, S., & Roth, M. J. (1990) *J. Virol. 64*, 6286−6290.

Sprous, D., Zacharias, W., Wood., Z. A., & Harvey, S. C. (1995) *Nucleic Acids Res. 23*, 1816−1821.
Tirado, M. M., & Garcia de la Torre, J. (1980) *J. Chem. Phys. 73*, 1986−1993.
Turchi, J. J., Huang, L., Murante, R. S., Kim, Y., & Bambara, R. A. (1994) *Proc. Natl. Acad. Sci. U.S.A. 91*, 9803−9807.
Varani, G., Cheong, C., & Tinoco, I. (1991) *Biochemistry 30*, 3280−3289.
Wang, A. C., Kim, S. G., Flynn, P. F., Sletten, E., & Reid, B. R. (1992a) *J. Magn. Reson. 100*, 358−366.
Wang, A. C., Kim, S. G., Flynn, P. F., Chou, S.-H., Orban, J., & Reid, B. R. (1992b) *Biochemistry 31*, 3940−3946.
Weiner, S. J., Kollman, P. A., Nguyen, D. T., & Case, D. A. (1986) *J. Comput. Chem. 7*, 230−252.
Whitcomb, J. M., Kumar, R., & Hughes, S. H. (1990) *J. Virol. 64*, 4903−4906.
Wyatt, J. R., & Walker, G. T. (1989) *Nucleic Acids Res. 17*, 7833−7842.
Zhu, L., & Reid, B. R. (1995) *J. Magn. Reson., Ser. B 106*, 227−235.
Zhu, L., Reid, B. R., Kennedy, M., & Drobny, G. P. (1994) *J. Magn. Reson., Ser. A 111*, 195−202.

BI9607822